

MICROSTRUCTURAL STABILITY AND MICROHARDNESS OF A CAST TiAl-BASED ALLOY FOR TURBINE BLADE APPLICATIONS

JURAJ LAPIN*, TATIANA PELACHOVÁ

The effect of ageing on the microstructural stability and microhardness of samples prepared from a cast turbine blade with nominal chemical composition Ti-46Al-2W-0.5Si (at.%) was studied. Ageing experiments were performed at three temperatures of 973, 1023, and 1073 K for various times ranging from 10 to 7300 h in air. Microstructure of the ageing samples consisted of lamellar, feathery and γ -rich regions. Microstructural analysis revealed that the lamellar regions are composed of α_2 (Ti₃Al) and γ (TiAl) lamellae, coarse B2 particles and fine needle-like B2 precipitates. The feathery regions contain γ -matrix with α_2 , B2 and Ti₅Si₃ particles. Coarse Ti₅Si₃ particles are identified within the γ -rich regions. During ageing the α_2 -phase in the lamellar and feathery regions transforms to the γ -phase and fine needle-like B2 precipitates. The microstructural instabilities lead to a softening of the alloy, which is characterized by a faster microhardness decrease of the lamellar regions comparing with that of the feathery ones. The measured time exponents and activation energies for softening are discussed from the point of diffusion-controlled transformations and coarsening of the coexisting phases. A possible effect of such microstructural changes on the kinetics of softening is analysed.

Key words: intermetallics, titanium aluminides, TiAl, heat treatment, microstructure, microhardness

MIKROŠTRUKTÚRNA STABILITA A MIKROTVRDOŠŤ ODLIEVANEJ INTERMETALICKEJ ZLIATINY NA BÁZE TiAl PRE TURBÍNOVÉ LOPATKY

Študovali sme vplyv starnutia na mikroštruktúrnú stabilitu a mikrotvrdošť vzoriek, ktoré sme pripravili z odlievanej turbínovej lopatky s nominálnym chemickým zložením Ti-46Al-2W-0,5Si (at.%). Starnutie sme vykonali na vzduchu pri teplotách 973, 1023 a 1073 K a pri rôznych časoch od 10 do 7300 h. Mikroštruktúra vzoriek pozostávala z lamelárnych oblastí, z oblastí s nepravidelnou (feathery) mikroštruktúrou a z oblastí bohatých na

Institute of Materials and Machine Mechanics, Slovak Academy of Sciences, Račianska 75, 831 02 Bratislava, Slovak Republic

* corresponding author, e-mail: ummslapi@savba.sk

fázu γ . Mikroštruktúrne analýzy ukázali, že lamelárne oblasti pozostávajú z lamiel fáz $\alpha_2(\text{Ti}_3\text{Al})$ a $\gamma(\text{TiAl})$, z hrubých častíc fázy B2 a z jemných precipitátov B2. Oblasti s nepravidelnou mikroštruktúrou sa skladajú z matrice γ , z častíc α_2 , B2 a z precipitátov Ti_5Si_3 . Oblasti bohaté na fázu γ obsahujú sférické precipitáty Ti_5Si_3 . V priebehu starnutia fáza α_2 transformuje na ihlicové precipitáty B2 a fázu γ . Mikroštruktúrne nestability zapríčiňujú zmäkčovanie zliatiny, ktoré je charakterizované rýchlejšim znižovaním mikrotvrdosti lamelárnych oblastí v porovnaní s oblasťami s nepravidelnou mikroštruktúrou. Namerané hodnoty časových exponentov a aktivačnej energie zmäkčovania analyzujeme z pohľadu difúziou riadených transformácií a hrubnutia fáz v priebehu starnutia. Zároveň analyzujeme možný vplyv týchto mikroštruktúrnych zmien na kinetiku zmäkčovania zliatiny.

1. Introduction

During the last decade, TiAl-based alloys have been extensively studied as potential high-temperature material in the gas turbine industry [1–3]. These alloys offer the opportunity for substantial weight savings when compared with Ni_3Al -based multiphase intermetallics or Ni-base superalloys assigned for similar structural applications [4–7]. Compared to Fe-base aluminides [8], TiAl-based alloys show significantly improved creep resistance in the temperature range from 973 to 1073 K [9]. In addition, they offer increased strength and improved creep, oxidation and burn resistance at high temperatures comparing with classical Ti-base alloys.

Several alloy compositions have been developed to meet specific property requirements of TiAl-based alloys: e.g. Ti-47Al-2Nb-2Cr (at.%) for maximum room temperature ductility [10] and Ti-46Al-2W-0.5Si (at.%) for maximum creep resistance [11]. Depending on chemical composition and heat treatments, TiAl-based alloys exhibit four different types of microstructures: near-gamma, duplex, nearly lamellar and fully lamellar microstructure [12–15]. The fully lamellar or nearly lamellar microstructure, consisting of the TiAl (γ -phase) and a small volume fraction of Ti_3Al (α_2 -phase), exhibits better creep resistance (apart from primary creep), higher fracture toughness and crack propagation resistance than duplex microstructure [16, 17]. On the other hand, higher tensile strength, ductility, and longer fatigue life are achieved for an alloy with duplex microstructure [16].

The largest proportion of usage of TiAl-based alloys is assumed to be in the gas turbine industry for turbine blades. As was shown in recent studies [14, 17], the microstructure of a large investment cast turbine blade after post-solidification thermo-mechanical treatment combined with subsequent heat treatments is not homogenous and changes from fully or nearly lamellar in the vicinity of the blade surface to duplex one in the central part. Although numerous studies were published on the microstructure of TiAl-based alloys, information about microstructural stability of large cast components like turbine blades at temperatures close to their operating temperature are still lacking in the literature. Therefore, evaluation of long-term microstructural stability of samples prepared from different regions of such large components is of great practical interest.

The aim of the present paper is to study the effect of the long-term ageing on the microstructural stability and microhardness of samples prepared from a large investment cast turbine blade with nominal chemical composition Ti-46Al-2W-0.5Si (at.%). The alloy was developed by Nazmy and Staubli [11] for investment cast turbine blades and turbocharger wheels with improved creep properties.

2. Experimental procedure

The intermetallic Ti-46Al-2W-0.5Si (at.%) alloy was provided by Alstom Ltd. in the form of investment cast turbine blade [14]. The as-received material was subjected to a hot isostatic pressing at an applied stress of 172 MPa and temperature of 1543 K for 4 h, which was followed by solution annealing at 1623 K for 1 h and gas fan cooling. The heat treatment was accomplished by stabilization annealing at 1273 K for 6 h and furnace cooling to room temperature.

Samples for ageing experiments with dimensions of $8 \times 8 \times 12$ mm were cut from the central part of the turbine blade by electro-spark machining. Selected positions in the turbine blade assured reproducible microstructure in all samples before ageing. Ageing experiments were performed at temperatures of 973, 1023, and 1073 K for various times ranging from 10 to 7300 h in air. After each ageing step the samples were cooled to room temperature at a cooling rate of $2 \text{ K}\cdot\text{s}^{-1}$. The Vickers microhardness measurements were performed at a load of 0.42 N on polished and slightly etched surfaces.

The microstructure evaluation was performed by optical microscopy (OM), scanning electron microscopy (SEM), transmission electron microscopy (TEM), and energy-dispersive X-ray (EDX) spectroscopy. OM and SEM samples were prepared using standard metallographic techniques and etched in a solution of 150 ml H_2O , 25 ml HNO_3 and 10 ml HF. The TEM samples were mechanically thinned to a thickness of about $50 \mu\text{m}$ and thinning was completed by ion milling. The volume fraction and size of coexisting phases were determined by computerized image analysis.

3. Results

3.1 Microstructure of the as-received material

Figure 1 shows the typical microstructure of the samples before ageing. The microstructure consists of lamellar (66 vol.%), feathery (26 vol.%) and γ -rich (8 vol.%) regions. The lamellar regions contain two types of lamellae: (1) continuous lamellae with apparently smooth interfaces and (2) discontinuous lamellae with precipitates. Figure 2a shows the typical TEM micrograph of the lamellar region with well-aligned α_2 (ordered Ti_3Al phase with D0_{19} crystal structure) and γ (ordered TiAl phase with L1_0 crystal structure) lamellae. Selected area diffraction (SAD) patterns from this region show crystallographic orientation relationships of $(0001)_{\alpha_2} \parallel \{111\}_{\gamma}$ and $\langle 11\bar{2}0 \rangle_{\alpha_2} \parallel \langle 1\bar{1}0 \rangle_{\gamma}$ between the coexisting phases, as seen

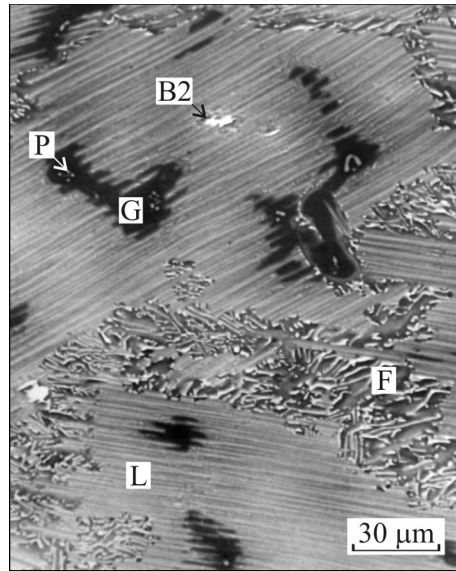


Fig. 1. Backscatter SEM micrograph showing typical microstructure of the samples before ageing: L – lamellar microstructure, F – feathery microstructure, G – γ -rich region, P – precipitates.

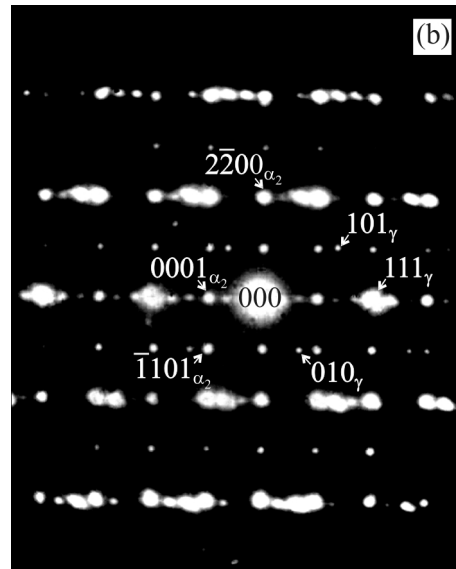
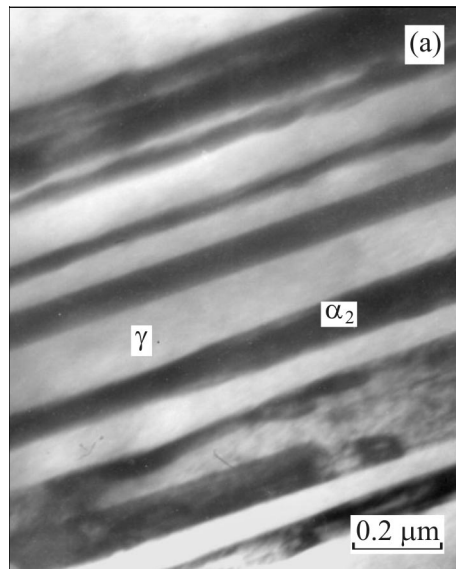


Fig. 2. (a) TEM micrograph showing continuous α_2 and γ lamellae in the lamellar region; (b) corresponding SAD pattern from the $[11\bar{2}0]_{\alpha_2} \parallel [\bar{1}01]_{\gamma}$ zone axis.

Fig. 3. TEM micrograph of discontinuous lamellae in the lamellar region.

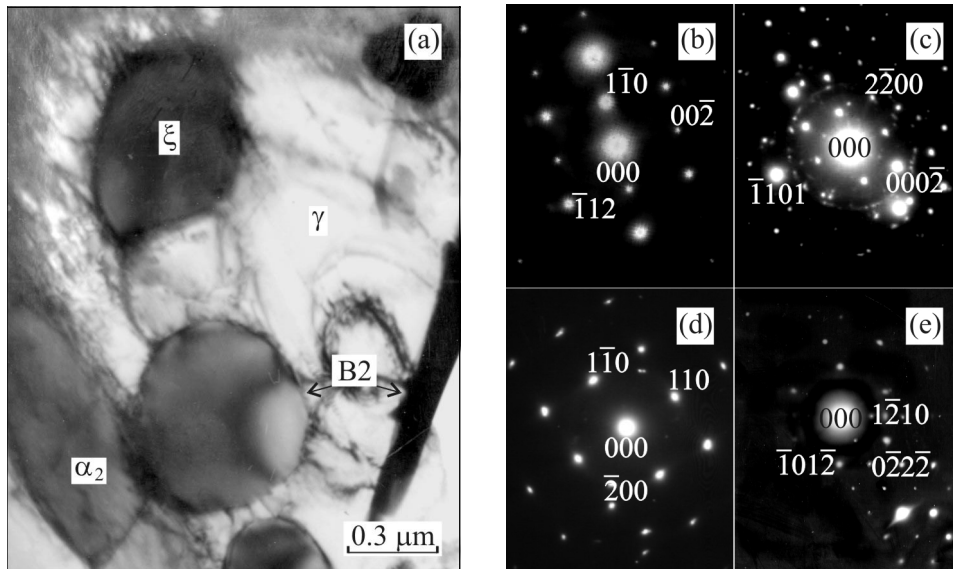
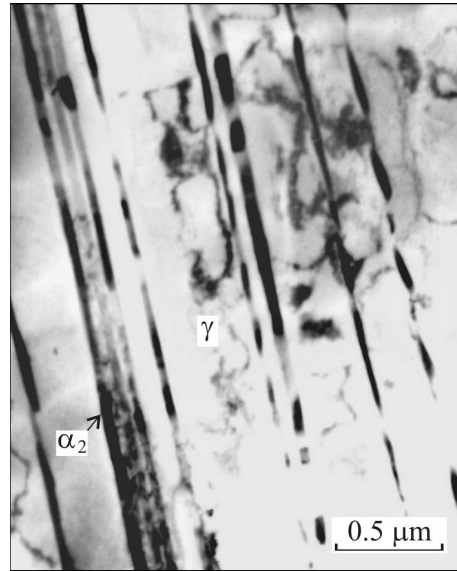


Fig. 4. (a) TEM micrograph showing the coexisting phases in the feathery region; (b) SAD pattern of the γ -phase from the $[110]_{\gamma}$ zone axis; (c) SAD pattern of the α_2 -phase from the $[11\bar{2}0]_{\alpha_2}$ zone axis; (d) SAD pattern of the B2-phase from the $[001]_{B2}$ zone axis; (e) SAD pattern of the $\xi(\text{Ti}_5\text{Si}_3)$ -phase from the $[10\bar{1}\bar{1}]_{\xi}$ zone axis.

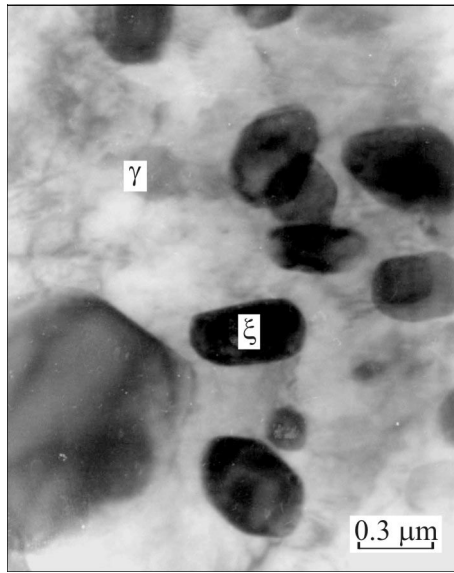


Fig. 5. TEM micrograph showing γ -rich region with $\xi(\text{Ti}_5\text{Si}_3)$ particles.

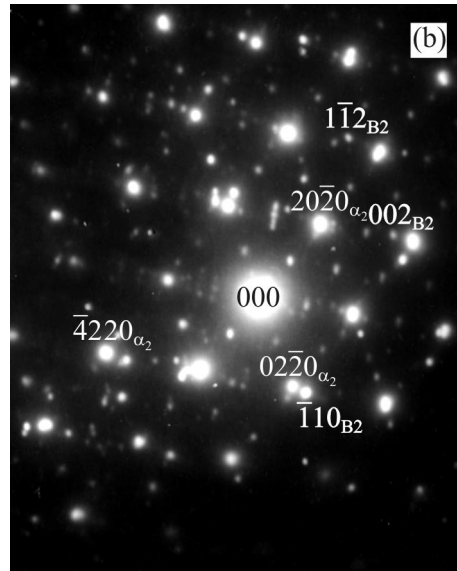
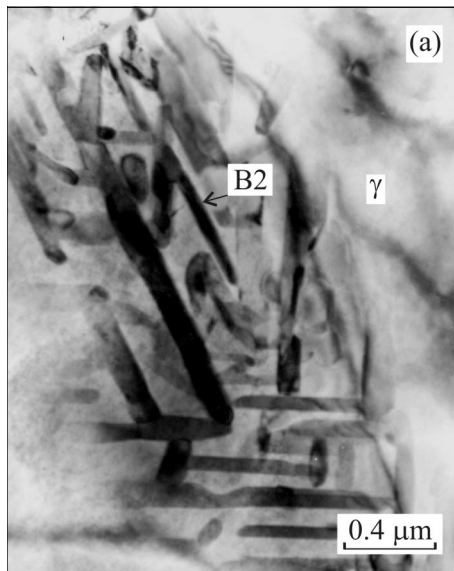


Fig. 6. (a) TEM micrograph showing transformation of the α_2 -lamellae to needle-like B2 precipitates and γ -matrix; (b) SAD pattern of B2 precipitates from the $[0001]_{\alpha_2} \parallel [\bar{1}\bar{1}0]_{\text{B2}}$ zone axis.

in Fig. 2b. The same crystallographic relationships were previously identified by Inui et al. [18] for a binary TiAl-based alloy. Yu et al. [19] identified numerous nanometer-scale B2 (ordered Ti-base solid solution) and Ti_5Si_3 precipitates at the apparently smooth α_2/γ interfaces using a high-resolution electron microscopy. Figure 3 shows TEM micrograph of the lamellar region containing discontinuous lamellae. Several authors [12, 20, 21] observed fine needle-like particles within discontinuous α_2 lamellae, which were identified to belong to B2-phase [12, 21]. In addition, some lamellar regions contain large blocky type B2 particles (1 vol.%) with an average size of about 20 μm (see Fig. 1).

Figure 4a shows TEM micrograph of the feathery region. The corresponding SAD patterns clearly indicate that the feathery region is composed of the γ -phase (Fig. 4b), irregular α_2 lamellae (Fig. 4c), B2 particles (Fig. 4d) and $\xi(\text{Ti}_5\text{Si}_3)$ precipitates (Fig. 4e).

Figure 5 shows TEM micrograph of the γ -rich region with spherical ξ precipitates. SAD patterns similar to that shown in Fig. 4e showed that these precipitates belong to Ti_5Si_3 -phase.

3.2 Microstructure after ageing

The microstructure of the aged samples observed by SEM was similar to that shown in Fig. 1. However, TEM observations showed that the as-received microstructure is unstable. During ageing the α_2 -phase in the lamellar and feathery regions transforms to the γ -phase and needle-like precipitates, as seen in Fig. 6a. The needle-like precipitates are identified to belong to B2-phase, as illustrated in Fig. 6b. On the contrary to the results recently reported by Gil et al. [12] and Muñoz-Morris et al. [22] for the samples aged at temperatures 1173–1273 K for ageing times ranging from 24 to 800 h, no notable globularization of the α_2 -phase and B2 precipitates within the lamellar or feathery regions was observed.

3.3 Effect of ageing on Vickers microhardness

Figures 7a and b show the variation of the Vickers microhardness of the lamellar and feathery regions with the ageing time, respectively. During ageing the microhardness of the lamellar and feathery regions decreases with increasing ageing time. It is clear from Fig. 7 that the softening is faster in the lamellar regions where the total microhardness decrease is higher. Since all microhardness values of the γ -rich regions (3.17 ± 0.05 GPa) fall within the error of the experimental measurements without any definite evolution with the ageing time, they are not included in Fig. 7. The kinetics of the softening process of the lamellar and feathery regions is analysed assuming time dependent equation in the form

$$\Delta HV_m = kt^m, \quad (1)$$

where ΔHV_m is the microhardness decrease, k is a material constant at a given temperature, t is the ageing time and m is the time exponent. Figures 8a and b

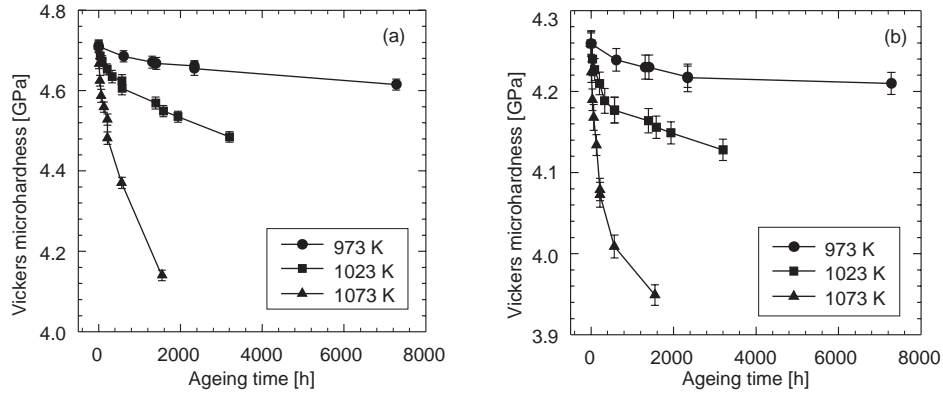


Fig. 7. Dependence of the Vickers microhardness on the ageing time: (a) lamellar regions; (b) feathery regions. The ageing temperatures are indicated in the figures.

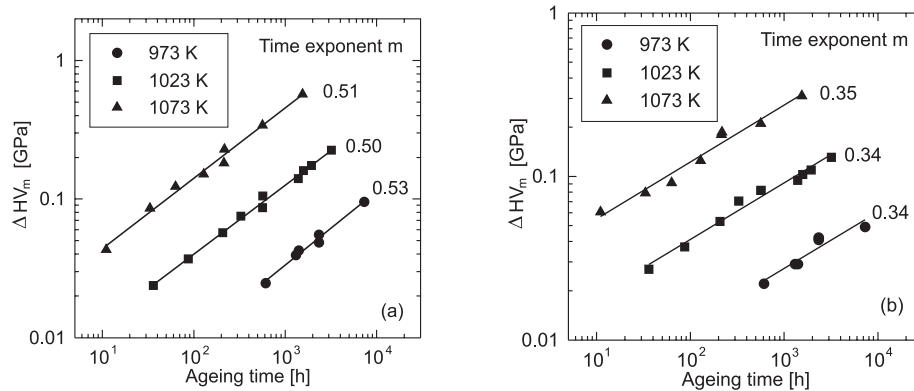
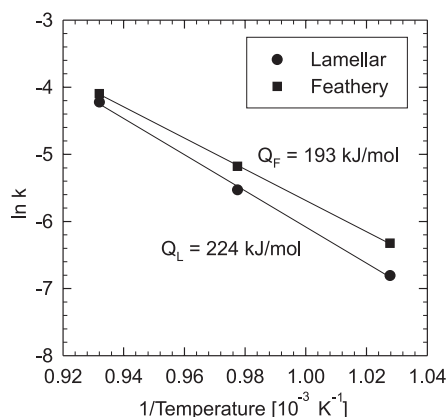


Fig. 8. Dependence of the microhardness decrease ΔHV_m on the ageing time: (a) lamellar regions; (b) feathery regions. The ageing temperatures are indicated in the figures.

show the evolution of the microhardness decrease ΔHV_m with the ageing time for the lamellar and feathery regions, respectively. The microhardness decrease ΔHV_m is calculated as a difference between the microhardness of the specific region before ageing and the microhardness after ageing for a given time. The linear regression analysis of the experimental data shown in Fig. 8 revealed that the average time exponent is $m = 0.51$ for the lamellar regions and $m = 0.34$ for the feathery ones. The correlation coefficients of these fits r^2 are better than 0.96. Similar time exponents of 0.5 for lamellar regions and 0.33 for feathery ones (designated as globular ones) were recently reported by Muñoz-Morris et al. [22] for Ti-46.5Al-

Fig. 9. Arrhenius diagram showing the dependence of the constant k on the inverse temperature. The type of regions is indicated in the figure.



-2W-0.5Si (at.%) alloy after ageing at 1173–1273 K up to 800 h. Taking the constants k obtained from the lines in Fig. 8, the activation energy for softening Q can be calculated according to equation

$$k = k_0 \exp\left(-\frac{Q}{RT}\right), \quad (2)$$

where k_0 is a material constant, R is the universal gas constant and T is the absolute temperature. Figure 9 shows the temperature dependence of the constant k on the inverse absolute temperature in the form of an Arrhenius diagram. From this figure, the activation energy for softening of the lamellar and feathery regions is calculated to be $Q_L = 224$ and $Q_F = 193$ kJ/mol, respectively. These values are significantly lower than those of 349 and 415 kJ/mol reported by Muñoz-Morris et al. [22] for the softening of the lamellar and feathery regions during ageing at 1173–1273 K, respectively. Our values of the activation energies for softening are also significantly lower than those for Al diffusion in TiAl or Ti₃Al of 360 and 395 kJ/mol, respectively [23, 24].

4. Discussion

In the lamellar regions, Muñoz-Morris et al. [22] related the microhardness decrease to an increase of interlamellar spacing λ . In the feathery regions, the microhardness decrease was related to an increase of free interparticle spacing L due to Ostwald ripening of globular α_2 and B2 particles. In both cases, the kinetics of the softening process was directly related to diffusion controlled transformations and coarsening of coexisting phases characterized by the activation energy for diffusion of Al in TiAl and Ti₃Al [22]. In spite of a general agreement that the kinetics of the interlamellar spacing increase and the particle coarsening can be controlled by diffusion of Al in TiAl or Ti₃Al, the precipitation strengthening is more complex problem. The precipitation strengthening includes several effective mechanisms (e.g. particle size, chemical, stacking-fault, modulus, coherency and

order strengthening mechanisms), which can operate simultaneously with various contributions to a final strength of the material [25]. For example, if Muñoz-Morris et al. [22] assumed that the free interparticle distance L follows with the ageing time a relationship $L \propto t^{0.33}$ and strengthening is assumed by Orowan mechanism according to a relationship $\Delta HV_m \propto 1/L$ then the time dependent microhardness decrease should follow a relationship $\Delta HV_m \propto t^{-0.33}$ and not $\Delta HV_m \propto t^{0.33}$. Similar analysis can be also performed for lamellar regions, where was clearly proved a linear relationship between the yield stress and the Vickers microhardness [26, 27]. A more complex analysis assuming time dependent phase transformations and coarsening mechanisms summarized by Philibert [28] and different strengthening mechanisms reviewed by Ardell [25] clearly show that the time dependent decrease of the microhardness cannot be directly related to diffusion controlled dissolution of the α_2 lamellae or coarsening of the particles. Therefore, the activation energy for softening may be significantly different from the activation energies for diffusion of specific elements in the alloy.

Comparing our values of the activation energy for softening of 224 and 193 kJ/mol with those of 349 and 415 kJ/mol reported by Muñoz-Morris et al. [22], one could see large discrepancies between these two works. The kinetics of the softening process can be described by an equation in the form

$$\Delta HV_m = k_0 t^m \exp\left(-\frac{Q}{RT}\right). \quad (3)$$

Figure 10a summarizes the microhardness decrease of the lamellar regions as a function of the ageing time normalized by the time exponent, the activation energy for softening of $Q_L = 224$ kJ/mol, the universal gas constant and the ageing temperature. It is clear that all present data clusters around a straight line. In addition, the experimental results reported by Muñoz-Morris et al. [22] for the softening of the lamellar regions can be also very well fitted using our value of the activation energy Q_L . The correlation coefficients r^2 of both fits are better than 0.97. On the other hand, two independent lines in Fig. 10a indicate that the softening kinetics for the same alloy during ageing at 973–1073 K (present work) differs from that at 1173–1273 K [22]. This difference can be explained by different state of the material before ageing. Muñoz-Morris et al. [22] subjected their as-received material to additional solution annealing at 1663 K for 1 h, which was followed by air-cooling to room temperature and subsequent ageing at temperatures ranging from 1173 to 1273 K. Such heat treatment resulted in a different microstructure composed only from lamellar and feathery regions before ageing. Figure 10b summarizes similar dependence of the microhardness decrease of the feathery regions on the ageing time normalized by the time exponent, the activation energy for softening of $Q_F = 193$ kJ/mol, the universal gas constant and the ageing temperature. As in the previous case, the experimental results reported for the softening of the feathery regions by Muñoz-Morris et al. [22] can be also very well fitted using our value of the activation energy Q_F . The correlation coefficients r^2 of both fits

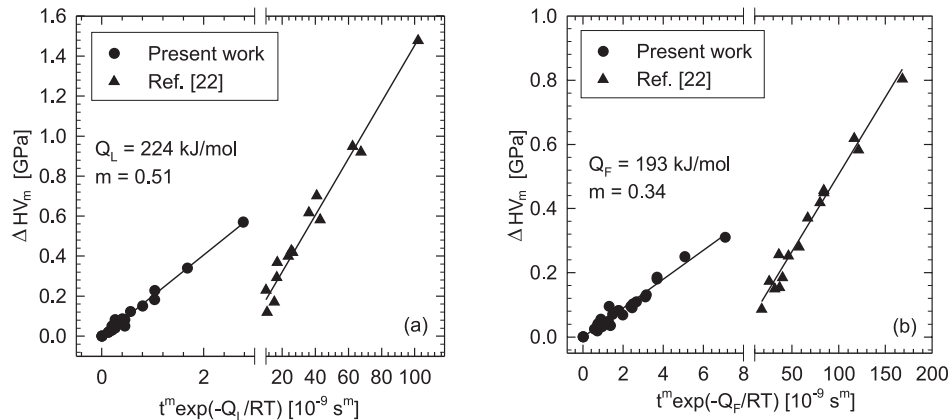


Fig. 10. Microhardness decrease ΔHV_m as a function of the ageing time normalized by the time exponent, the activation energy for softening, the universal gas constant and the absolute temperature: (a) lamellar regions; (b) feathery regions. The type of the experimental data is indicated in the figures.

are better than 0.98. It should be emphasized that we performed the same analysis using the activation energies for softening of 349 and 415 kJ/mol [22]. For both lamellar and feathery regions, such analysis does not result in a single line for the experimental data reported by Muñoz-Morris et al. [22] or for our data (each ageing temperature gives independent line). This indicates that the values of the activation energies for softening reported by Muñoz-Morris et al. [22] are somehow overestimated and cannot describe the softening kinetics of the alloy according to Eq. (3) over the studied temperature range.

5. Conclusions

The effect of long-term ageing on the microstructural stability and microhardness of samples prepared from a large investment cast turbine blade with nominal chemical composition Ti-46Al-2W-0.5Si (at.%) was studied. The following conclusions are reached:

1. Before ageing the microstructure consists of lamellar, feathery and γ -rich regions. The lamellar regions are composed of α_2 and γ lamellae, coarse B2 particles and fine needle-like B2 precipitates. The feathery regions contain γ -matrix with α_2 , B2 and Ti_5Si_3 particles. Coarse Ti_5Si_3 particles are identified within the γ -rich regions.
2. The as-received microstructure is unstable. The α_2 -phase in the lamellar and feathery regions transforms to the γ -phase and needle-like B2 precipitates during ageing at temperatures ranging from 973 to 1073 K.
3. The microstructural instabilities lead to a softening of the alloy. The microhardness decrease is faster in the lamellar regions than in the feathery ones. The

average time exponent of the microhardness decrease is determined to be 0.51 and 0.34 and the activation energy for softening is calculated to be 224 and 193 kJ/mol for the lamellar and feathery regions, respectively.

4. The kinetics of the softening process cannot be directly related to diffusion controlled transformations and coarsening of the coexisting phases but is much more complex. The activation energy for softening can be significantly different from that for the diffusion of specific elements in the alloy.

Acknowledgements

This article is dedicated to Prof. Dr. P. Kratochvíl, DrSc., on the occasion of his 70th birthday. The authors gratefully acknowledge the financial support of the Slovak Grant Agency for Science under the contract VEGA 2/4166/24. They also express their thanks to Dr. M. Nazmy from ALSTOM Ltd. for providing the experimental material.

REFERENCES

- [1] SMARSLY, W.—BAUR, F.—GLITZ, G.—CLEMENS, H. —KHAN, T.—THOMAS, M.: In: *Structural Intermetallics 2001*. Eds.: Hemker, K. J., Dimiduk, D. M., Clemens, H., Darolia, R., Inui, H., Larsen, J. M., Sikka, V. K., Thomas, M., Whittenberger, J. D. TMS, Warrendale, PA 2001, p. 25.
- [2] NAZMY, M.—LUPINC, V.: In: *Materials for Advanced Power Engineering 2002*. Eds.: Lecomte-Beckers, J., Carton, M., Schubert, F., Ennis, P. J. Forschungszentrum Jülich GmbH, Vol. 21, Part I, 2002, p. 43.
- [3] DIMIDUK, D. M.: *Mater. Sci. Eng. A*, 263, 1999, p. 281.
- [4] LAPIN, J.: *Kovove Mater.*, 40, 2002, p. 209.
- [5] FLORIAN, M.: *Kovove Mater.*, 41, 2003, p. 73.
- [6] SKLENIČKA, V.—KUDRMAN, J.—KUCHAŘOVÁ, K.—DANĚK, R.—HRBÁČEK, K.: *Kovove Mater.*, 40, 2002, p. 11.
- [7] MALDINI, M.—LUPINC, V.—ANGELLA, G.: *Kovove Mater.*, 42, 2004, p. 21.
- [8] KRATOCHVÍL, P.—ŠEDIVÁ, I.—HAKL, J.—VLASÁK, T.: *Kovove Mater.*, 40, 2002, p. 124.
- [9] LAPIN, J.: *Scripta Mater.*, 50, 2004, p. 261.
- [10] BHOWAL, P. R.—MERRICK, H. F.—LARSEN, D. E.: *Mater. Sci. Eng. A*, 192/193, 1995, p. 685.
- [11] NAZMY, M. —STAUBLI, M.: U. S. Pat. # 5,207,982 and European Pat. # 45505 BI.
- [12] GIL, I.—MUÑOZ-MORRIS, M. A.—MORRIS, D. G.: *Intermetallics*, 9, 2001, p. 373.
- [13] RECINA, V.—AHLSTRÖM, J.—KARLSSON, B.: *Mater. Charact.*, 38, 1997, p. 287.
- [14] LAPIN, J.—KLIMOVÁ, A.: *Kovove Mater.*, 41, 2003, p. 1.
- [15] LAPIN, J.—ONDRŮŠ, Ľ.: *Kovove Mater.*, 40, 2002, p. 161.
- [16] RECINA, V.—LUNDSTRÖM, D.—KARLSSON, B.: *Metall. Mater. Trans.*, 33A, 2002, p. 2869.
- [17] LAPIN, J.—PELACHOVÁ, T.: In: *Materials for Advanced Power Engineering 2002*. Eds.: Lecomte-Beckers, J., Carton, M., Schubert, F., Ennis, P. J. Forschungszentrum Jülich GmbH, Vol. 21, Part II, 2002, p. 623.

- [18] INUI, H.—NAKAMURA, A.—OH, M. H.—YAMAGUCHI, M.: *Ultramicroscopy*, 39, 1991, p. 268.
- [19] YU, R.—HE, L. L.—CHENG, Z. Y.—ZHU, J.—YE, H. Q.: *Intermetallics*, 10, 2002, p. 661.
- [20] LAPIN, J.—KLIMOVÁ, A.—PELACHOVÁ, T.: *Scripta Mater.*, 49, 2003, p. 681.
- [21] YIN, W. M.—LUPINC, V.—BATTEZZATI, L.: *Mater. Sci. Eng. A*, 239-240, 1997, p. 713.
- [22] MUÑOZ-MORRIS, M. A.—FERNÁNDEZ, I. G.—MORRIS, D. G.: *Scripta Mater.*, 46, 2002, p. 617.
- [23] HERZIG, CH.—PRZEORSKI, T.—MISHIN, Y.: *Intermetallics*, 7, 1999, p. 389.
- [24] RÜSING, J.—HERZIG, CH.: *Intermetallics*, 4, 1996, p. 647.
- [25] ARDELL, A. J.: *Metall. Trans. A*, 16A, 1985, p. 2131.
- [26] LAPIN, J.: *J. Mater. Sci. Lett.*, 22, 2003, p. 747.
- [27] LAPIN, J.—ONDRŮŠ, L.—BAJANA, O.: *Mater. Sci. Eng. A*, 360, 2003, p. 85.
- [28] PHILIBERT, J.: *Atom Movements Diffusion and Mass Transport in Solids*. Les Editions de Physique, Les Uli 1991, p. 421.

Received: 19.3.2004